

Fully directional quantum-limited phase-preserving amplifier

G. Liu,^{1,*†,**} A. Lingenfelter^{1,2,**} V.R. Joshi,¹ N.E. Frattini,^{1,§} V.V. Sivak,^{1,¶} S. Shankar^{1,||} and M.H. Devoret^{1,†}

¹*Department of Applied Physics, Yale University, New Haven, Connecticut 06520, USA*

²*Department of Physics, University of Chicago, Chicago, Illinois 60637, USA*

(Received 8 May 2023; revised 14 October 2023; accepted 18 December 2023; published 12 January 2024)

We present a way to achieve fully directional, quantum-limited phase-preserving amplification in a four-port, four-mode superconducting Josephson circuit by utilizing interference between six parametric processes that couple all four modes. Full directionality, defined as the reverse isolation surpassing forward gain between the matched input and output ports of the amplifier, ensures its robustness against impedance mismatch that might be present at its output port during applications. Unlike existing directional phase-preserving amplifiers, both the minimal backaction and the quantum-limited added noise of this amplifier remains unaffected by noise incident on its output port. In addition, the matched input and output ports allow direct on-chip integration of these amplifiers with other circuit QED components, facilitating scaling up of superconducting quantum processors.

DOI: 10.1103/PhysRevApplied.21.014021

I. INTRODUCTION

Directional, quantum-limited signal amplification belongs to the cadre of basic quantum information-processing tasks. In superconducting circuits, it is commonly performed by a combination of ferrite-based circulators and reflection Josephson parametric amplifiers [1–4]. Even though these amplifiers work very close to the quantum limit, photon loss in circulators and other associated components in the signal pathway significantly reduce the quantum efficiency of this amplification process. Furthermore, the strong magnetic field needed for the operation of ferrite-based circulators and their bulkiness make them difficult to integrate with superconducting circuits. Therefore, a question naturally arises: is it possible to achieve directional quantum-limited amplification without using ferrite-based circulators?

In recent theoretical works by Ranzani *et al.* [5,6], it is shown that in a parametrically coupled system, nonreciprocity can be generated from the dissipation of ancillary

modes and the interference of multiple coupling paths that connect the input mode to the output mode. Following this concept, both phase-preserving and phase-sensitive directional quantum-limited Josephson parametric amplifier have been demonstrated [7–11]. Meanwhile, Metelmann *et al.* have shown that any coherent coupling can be made directional by balancing it with a dissipative process [12,13]. This method has been employed in the demonstration of nonreciprocity in both optical domain and microwave domain with optomechanics [14–22].

However, in these directional amplifiers, there is either unity transmission in the reverse direction or amplification in reflection from the output port [7–10,13,20,23]. To ensure that only vacuum noise goes back to the signal source (i.e., minimal backaction) and that only quantum-limited noise is added to the output signal, it requires that only vacuum noise can enter the output port of the amplifier. Unfortunately, this is hardly the case in experiments; the amplifier output port is typically connected to parts of the apparatus, which are thermalized at temperatures much higher than the vacuum noise effective temperature of the frequency band of interest. Thermal photons are then emitted towards the directional amplifier, leading to unwanted backaction and added noise. Therefore, it is desirable to build a directional amplifier with matched input and output ports, as well as sufficient reverse isolation between them. Of note, the reverse isolation needs to exceed the forward gain. This ensures robustness of its minimal backaction and quantum-limited noise performances against any impedance mismatch and noise that might be present on its output port during applications. We

*gangqiang.liu@yale.edu

†michel.devoret@yale.edu

‡Present address: Quantum Circuits, Inc., 25 Science Park, New Haven, CT 06511, USA.

§Present address: Nord Quantique, Sherbrooke, Québec, J1J 2E2, Canada.

¶Present address: Google Quantum AI, Santa Barbara, CA, USA.

||Present address: Electrical and Computer Engineering, University of Texas, Austin, TX, USA.

**These authors contributed equally.

call such amplifiers the *fully* directional quantum-limited amplifiers.

In this work, we show that fully directional quantum-limited phase-preserving amplifiers can be built with four-port four-mode systems that have properly arranged two-mode squeezing and frequency-conversion couplings between the modes. To reach this result, we first derive the minimum scattering matrices of fully directional quantum-limited phase-preserving amplifiers. We find that there exists two such scattering matrices, which represent four-port systems. From these scattering matrices, we then generate the coupling matrices between the modes. These coupling matrices in turn provide the full implementation guideline for these amplifiers. We also theoretically investigate the performance of these amplifiers under practical operating conditions and find they are robust against imperfection in parametric couplings and input signal detuning.

II. MINIMAL SCATTERING MATRIX OF A FULLY-DIRECTIONAL QUANTUM-LIMITED AMPLIFIER

We start with the scattering matrix representation of a linear amplifier. For a linear amplifier with N ports, the input and output signals are related by

$$\begin{bmatrix} a_1^{\text{out}} \\ a_1^{\text{out}\dagger} \\ \vdots \\ a_N^{\text{out}} \\ a_N^{\text{out}\dagger} \end{bmatrix} = \tilde{S} \begin{bmatrix} a_1^{\text{in}} \\ a_1^{\text{in}\dagger} \\ \vdots \\ a_N^{\text{in}} \\ a_N^{\text{in}\dagger} \end{bmatrix}, \quad (1)$$

where a_n^{in} ($a_n^{\text{in}\dagger}$) and a_n^{out} ($a_n^{\text{out}\dagger}$) are field operators of the input and output signals on the n th port of the amplifier, and \tilde{S} is the $2N$ -by- $2N$ scattering matrix. The reason for separating a and a^\dagger for each port is that the amplifier might not a priori amplify the two quadratures by the same coefficient.

The requirement for performing fully directional quantum-limited phase-preserving amplification with such an amplifier translates into the following requirements on its scattering matrix.

(i) The scattering matrix can always be block-diagonalized on a proper mode basis,

$$L\tilde{S}L^{-1} = \begin{bmatrix} S & 0 \\ 0 & S^* \end{bmatrix}, \quad (2)$$

where L is the linear transformation from the mode basis in Eq. (1) to the proper one, S is a N -by- N matrix, which is often referred to as the scattering matrix even

though it might mix a_n and a_m^\dagger . The property of these two submatrices being conjugate ensures phase-preserving amplification. In the graph-based notation of the scattering matrix [6,24], this property ensures that the full graph can be decomposed into two subgraphs.

(ii) The scattering matrix is symplectic,

$$\tilde{S}^T \cdot J \cdot \tilde{S} = J, \quad (3)$$

where J is the symplectic matrix

$$J = \begin{bmatrix} 0 & 1 & & & \\ -1 & 0 & & & \\ & & \ddots & & \\ & & & 0 & 1 \\ & & & -1 & 0 \end{bmatrix}. \quad (4)$$

The meaning of Eq. (3) is that the device preserves the information content of the input signal, or in other words, it preserves the commutation relation of the input field operators [25].

(iii) The subscattering matrix between the input port (port 1) and output port (port 2) should take the form

$$[S]_{1,2} = \begin{bmatrix} 0 & 0 \\ \sqrt{G}e^{i\phi} & 0 \end{bmatrix}, \quad (5)$$

where $S_{21} = \sqrt{G}e^{i\phi}$ is the gain from the input to the output port. This stipulates that both the input and output ports are matched, and the reverse isolation ($1/|S_{12}|$) is infinity.

(iv) Scattering matrix elements that couple other ports to the input and output ports should satisfy the following condition:

$$\sum_{p=3}^N |S_{1p}|^2 = 1, \quad \sum_{p=3}^N |S_{2p}|^2 \approx G \quad \text{for } G \gg 1, \quad (6)$$

such that both the backaction and added noise of the amplifier are quantum-limited when only vacuum noise enters the output port and all other auxiliary ports.

With this set of conditions, we obtain equations for the N^2 complex scattering matrix elements of S . In solving these equations (see Sec. A within the Supplemental Material [26]), we find that solutions exist only for $N \geq 4$. Therefore, at least four ports—input port, output port, and two ancillary ports—are needed to perform fully directional quantum-limited phase-preserving amplification. Henceforth, we refer to S as the scattering matrix and \tilde{S} as the full scattering matrix.

For a four-port system, we find that there exist two types of such four-by-four scattering matrices. We name the corresponding four-port fully directional amplifiers (4PFDAs)

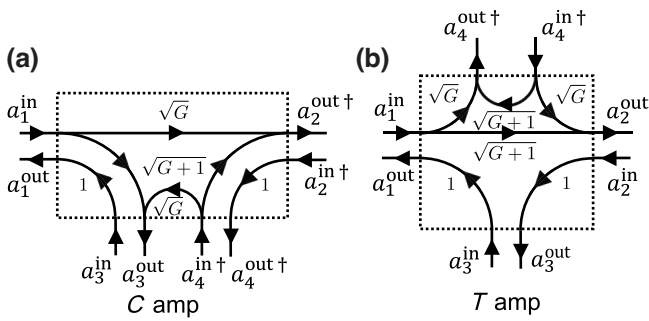


FIG. 1. Scattering graphs of the two four-port fully directional amplifiers nicknamed *C* amp and *T* amp. (a) *C* amp has a “*cis*” configuration of the ancillary ports meaning they are on the same side of the wave trajectory from port 1 to port 2, and (b) *T* amp has a “*trans*” configuration of the ancillary ports meaning they are on the opposite side of the wave trajectory from port 1 to port 2. Scattering matrix elements between two ports are represented by lines with the arrow indicating wave-trajectory direction between ports. The value of the scattering matrix elements is shown next to the line.

as *cis* and *trans* amplifier (*C* amp and *T* amp) based on the “topology” of their scattering graph (see Fig. 1), respectively. Minimal form of these scattering matrices are, for the *C* amp

$$S_C = \begin{bmatrix} 0 & 0 & 1 & 0 \\ \sqrt{G} & 0 & 0 & \sqrt{G+1} \\ \sqrt{G+1} & 0 & 0 & \sqrt{G} \\ 0 & 1 & 0 & 0 \end{bmatrix} \quad (7)$$

and for the *T* amp

$$S_T = \begin{bmatrix} 0 & 0 & 1 & 0 \\ \sqrt{G+1} & 0 & 0 & \sqrt{G} \\ 0 & 1 & 0 & 0 \\ \sqrt{G} & 0 & 0 & \sqrt{G+1} \end{bmatrix}, \quad (8)$$

where $G \geq 0$. The corresponding mode bases are

$$A_C^{\text{in,out}} = \begin{bmatrix} a_1 \\ a_2^\dagger \\ a_3 \\ a_4^\dagger \end{bmatrix}^{\text{in,out}}, \quad A_T^{\text{in,out}} = \begin{bmatrix} a_1 \\ a_2 \\ a_3 \\ a_4^\dagger \end{bmatrix}^{\text{in,out}}, \quad (9)$$

respectively. Note the matrices have been made positive and real after a change of phase of the incoming and outgoing waves. In general, scattering matrices depend on input signal frequency while Eqs. (7) and (8) represent the special case of resonant input signal. These two scattering matrices are graphically represented in Fig. 1.

There are differences between these two types of amplifiers, although both provide same scattering relation between the input and output ports in the high gain limit ($G \gg 1$). First, all ports of *C* amp are matched while *T* amp has one ancillary port with reflection gain. Second, from the mode basis, one notices that the conjugate frequency components of the input and output are coupled in *C* amp while the same frequency components are coupled in *T* amp. The two auxiliary ports play crucial roles: when they are terminated with matched cold load, they serve as “dumps” for signal entering the device from the output port, therefore providing isolation from output port to input port. Meanwhile, their conjugation also provides vacuum noise going to the input port as required for minimum quantum backaction.

III. MODE COUPLING OF THE 4PFDA

With the minimal scattering matrices determined, we now discuss how to obtain these scattering matrices from a coupled-mode system. In general, there can be more modes than ports in such systems, which becomes necessary when engineering to increase the bandwidth of the amplifier [24]. We focus here on the case of minimal number of required modes. We therefore consider an N -port N -mode system. The scattering matrix of such a system is given by its coupling to the environment and between the modes as (see derivation within the Supplemental Material [26])

$$S = (\Sigma + M)^{-1}(\Sigma - M), \quad (10)$$

with

$$\Sigma = \begin{bmatrix} \kappa_1/2 & & & \\ & \ddots & & \\ & & \ddots & \\ & & & \kappa_N/2 \end{bmatrix}, \quad (11)$$

which represents the amplitude damping rate of the modes due to their coupling to the environment, and

$$M = \begin{bmatrix} i\Delta_1 & M_{12} & \cdots & M_{1N} \\ M_{21} & i\Delta_2 & \cdots & M_{2N} \\ \vdots & \vdots & \ddots & \vdots \\ M_{N1} & M_{N2} & \cdots & i\Delta_N \end{bmatrix}, \quad (12)$$

which represents the coupling between the modes (M_{mn}) and to the external drives ($i\Delta_n$) with $\Delta_n = \omega_n^{\text{in}} - \omega_n$. Equation (10) can be viewed as the generalized reflection coefficient between two systems of different impedances. Given the scattering matrix S , one can obtain the coupling between the modes from Eq. (10) as

$$M = \Sigma(I - S)(I + S)^{-1}, \quad (13)$$

where I is the identity matrix.

From the scattering matrices given in Eqs. (7) and (8), we obtain the coupling Hamiltonians of these two amplifiers as

$$H_C/\hbar = \frac{1}{2} \left(g_{12}a_1a_2 + g_{13}a_1a_3^\dagger + g_{14}a_1a_4 + g_{23}a_2a_3 + g_{24}a_2a_4^\dagger + g_{34}a_3a_4 \right) + \text{h.c.}, \quad (14)$$

$$H_T/\hbar = \frac{1}{2} \left(g_{12}a_1a_2^\dagger + g_{13}a_1a_3 + g_{14}a_1a_4 + g_{23}a_2a_3^\dagger + g_{24}a_2a_4 + g_{34}a_3a_4^\dagger \right) + \text{h.c.}, \quad (15)$$

where

$$g_{mn} = \pm i\sqrt{\kappa_m\kappa_n} \frac{\sqrt{G-1}}{\sqrt{G+1}} \quad (16)$$

for terms with $a_m a_n$, and

$$g_{mn} = \pm i\sqrt{\kappa_m\kappa_n} \quad (17)$$

for terms with $a_m a_n^\dagger$, which correspond to *two-mode squeezing* and *frequency conversion* between the modes, respectively. The sign of each term, i.e., the phase of each coupling, is uniquely determined by the scattering matrix. The two-mode squeezing coupling with the coupling rate in Eq. (16) alone leads to phase-preserving amplification of input signals to the two modes with photon-number gain of G in reflection ($G - 1$ in transmission). The frequency conversion coupling with coupling rate in Eq. (17) leads to *perfect* photon conversion, henceforth denoted as $C = 1$, between the two modes. More generally, the photon conversion efficiency C is related to the coupling rate in Eq. (17) through an additional prefactor $\sqrt{C}(1 + \sqrt{1 - C})^{-1}$ on the right-hand side Eq. (17).

These coupling Hamiltonians are graphically illustrated in Fig. 2. First, one notices that the total phases of the three couplings associated with each mode is either $\pi/2$ or $-\pi/2$. Furthermore, each closed loop of three coupled modes forms a three-port directional amplifier or circulator, which have been demonstrated in previous works [7,8,16,18,22]. In fact, the coupling graphs of the C amp and T amp are equivalent to the two different ways of connecting a three-port directional amplifier to a three-port circulator. See the Supplemental Material [26] for more detailed discussion.

In Ref. [13], a four-port four-mode system with five couplings was proposed for quantum-limited directional phase-preserving amplification. However, the input port of such a system would produce unity reflection, which is undesired. Such reflection could lead to unwanted backaction on the signal source. Therefore, the four-port four-mode system with six properly arranged couplings presented here represents the minimum construction of a

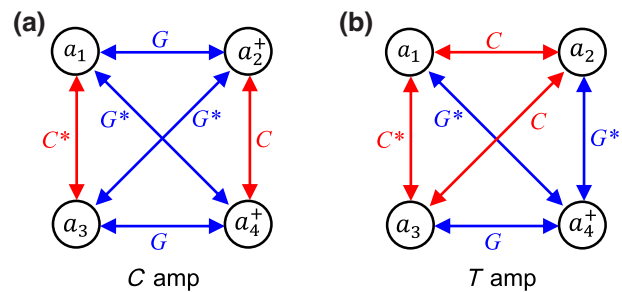


FIG. 2. All-parametric implementation of the two four-port fully directional amplifiers in Fig. 1. (a) Parametric coupling graph of C amp. There are three conversion couplings (C or C^* , red) and three gain couplings (G or G^* , blue). (b) Parametric coupling graph of T amp. There are two conversion couplings and four gain couplings. The phase of each individual coupling is either $\pi/2$ for C and G , or $-\pi/2$ for C^* and G^* .

fully directional quantum-limited phase-preserving amplifier. On the other hand, as shown in Ref. [27], a fully directional phase-sensitive amplifier would require a three-port three-mode system with five couplings.

IV. EFFECTS OF IMPERFECT CONVERSION IN 4PFDA

So far, we have discussed only the performance of these amplifiers under ideal situation: perfect frequency conversion and resonant input signal. In this section, we will show that even under practical operating conditions—imperfect frequency conversion and detuned input signal—these amplifiers give superior performance compared to existing directional amplifiers based on interference between multiple parametric processes.

First of all, we investigate the effect of imperfection in frequency conversion between the modes on the performance of the amplifiers. In general, with imperfect conversion ($C < 1$) there will be reflection on the input and output ports. In Fig. 3, we show the scattering matrix elements between the input and output ports of the C amp and T amp versus phase-preserving gain (G) for frequency conversion of $C = 0.99$ and $C = 0.999$ between each pair of modes, which are readily achievable in experiments.

For C amp [Fig. 3(a)], both reflection (S_{11} , S_{22}) and transmission in reverse direction (S_{12}) increases as the gain coupling between paired modes increases, and eventually saturates in high gain limit ($G > 40$ dB). As expected, better amplification in forward direction (S_{21}) and isolation in reverse direction (S_{12}) are achieved with better conversion between the modes. With readily achievable conversion of $C = 0.99$ between modes, this amplifier is matched at the -15 -dB level on both input and output port while providing 20-dB forward gain. To achieve this level of input matching and gain with a single-parametric reflection amplifier, at least two circulators are needed in front of the amplifier.

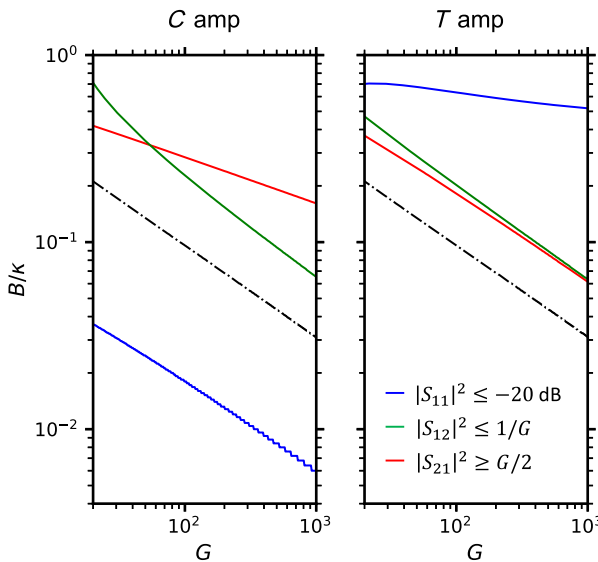


FIG. 3. Scattering matrix elements of C amp and T amp for imperfect conversion. Input and output matching (S_{11} and S_{22} , blue), forward gain (S_{21} , red) and reverse isolation (S_{12} , green) for C amp in panel (a), and for T amp in panel (b) with respect to gain of single coupling (G) for $C = 0.99$ (dashed) and $C = 0.999$ (dotted).

For T -amp [Fig. 3(b)], we observe very different behaviors. Both the reflections and forward gain start to increase rapidly as gain coupling between the paired modes increases above $4/(1 - C)$. However, impedance matching of both the input and output ports remain better than -20 dB while the forward gain approaches 20 dB. This performance can be readily achieved with phase-preserving gain of 17 dB between the coupled modes for both frequency conversion values. Furthermore, the isolation in reverse direction is insensitive to the phase-preserving gain strength.

V. FREQUENCY DEPENDENCE OF 4PFDA PERFORMANCE

Now we show the amplifier performance for detuned input signal. The scattering matrix for detuned input signal is derived from the Hamiltonian of the amplifiers together with Eq. (10). As shown within the Supplemental Material [26], they are complex functions of the signal detuning. In Fig. 4, we show the four scattering matrix elements between the input and output ports for frequency conversion strengths $C = 1$ and $C = 0.99$, while keeping the forward gain $|S_{21}|^2 = 20$ dB for resonant input signal. Without losing generality, we assume all modes have the same linewidth κ .

The most striking difference between these two amplifiers is the frequency dependence of their matching conditions (top row of Fig. 4). For C amp, impedance matching rapidly degrades with signal detuning. For T amp, good

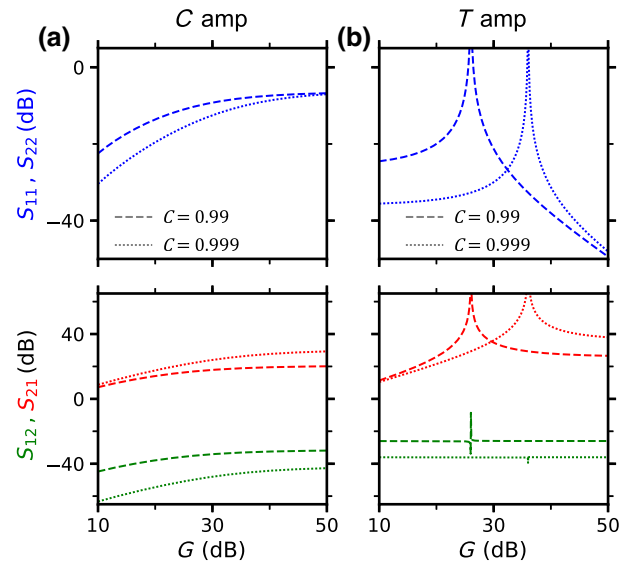


FIG. 4. Frequency dependence of scattering matrix elements of C amp and T amp. Input and output matching (S_{11} and S_{22} , blue), forward gain (S_{21} , red) and reverse isolation (S_{12} , green) of C amp in (a), and T amp in (b) with respect to reduced detuning Δ/κ . Solid lines represent results for the case with gain couplings of $G = 20$ dB and conversion couplings of $C = 1$ between the modes. Dashed lines in (a) represent results for gain couplings of $G = 23$ dB and conversion couplings of $C = 0.999$. Dashed lines in (b) represent results for gain couplings of $G = 20$ dB and conversion couplings of $C = 0.99$. Note that in C amp, much higher phase-preserving gain between modes would be needed for 20-dB forward gain if $C = 0.99$ instead of 0.999 .

impedance matching can be achieved over a much larger range of detuning. The robustness of impedance matching over signal detuning in T amp comes from the fact that two of three parametric processes that input and output modes directly participate are frequency conversions, which diminish reflections. In contrast, in C amp two of these three parametric processes are amplifications, which generate amplified signal in reflection.

Forward gain and reverse isolation of these two amplifiers have similar frequency dependence (bottom row of Fig. 4), except that better reverse isolation is achieved in C amp for near-resonance signal. Overall, T amp appears to be easier to operate as it requires less gain and conversion to achieve the same forward gain as C amp.

VI. BANDWIDTH OF 4PFDA

A useful metric for characterizing the frequency-dependent performance of an amplifier is its bandwidth, which is typically defined as the frequency range over which its gain drop by 3 dB from the desired value. For a resonator-based single-pump amplifier, such as the two-port, two-mode phase-preserving amplifier, its bandwidth (B) is related to the geometric mean of the linewidth of its

two modes ($\bar{\kappa}$) and gain by the relation $\bar{\kappa} \approx B\sqrt{G}$, which is known as the fixed gain-bandwidth product [28].

For amplifiers involving multiple parametric processes such as the *C* amp and *T* amp, because multiple scattering parameters are relevant to their applications, their bandwidth should be defined as the frequency range over which *all* these scattering parameters maintain desired performance. In these two amplifiers, all four scattering parameters between the input and output ports are relevant. Therefore, we define the bandwidth of the them as the frequency range over which *all the following conditions are satisfied*: $|S_{11}|^2, |S_{22}|^2 \leq 0.01$, $|S_{12}|^2 \leq 1/G$, $|S_{21}|^2 \geq G/2$, where G is the forward gain for resonant input signal.

The chosen requirement on input match is on par with that of commercially available circulators that are widely used in circuit-QED experiments [29,30]. The requirement on reverse isolation, where $|S_{12}|^2 \leq 1/G$, is to prevent the formation of a positive feedback loop caused by reflections from downstream components and the signal source, which can return the amplifier output to its input. The extreme case of full reflection from downstream components has been considered here to obtain the lower bound of this reverse isolation bandwidth. In addition, the reverse isolation provides protection to the signal source against reflected signal and noise originating from these downstream components. It is worthwhile to note that the specific level of reverse isolation required varies depending

on the signal source's susceptibility to such disturbances, making it inherently application dependent. Therefore, the bandwidth for reverse isolation is defined with respect to the aforementioned situation.

In Fig. 5, we show the bandwidth defined by each of these conditions versus forward gain. For *C* amp, the bandwidth determined by impedance-matching condition, which is nearly 10 times narrower than those determined by forward gain and reverse isolation, defines the amplifier bandwidth. For *T* amp, the 3-dB bandwidth of forward gain defines the amplifier bandwidth. For both amplifiers, their 3-dB bandwidths of forward gain are approximately twice of the 3-dB bandwidth of a resonator-based single-parametric amplifier such as JPAs (dash-dotted line), while their scaling with gain are similar. Overall, for most applications the *T* amp appears to be a more favorable configuration.

VII. CONCLUSION

In summary, we have presented two fully directional quantum-limited phase-preserving parametric amplifiers, which have matched input and output ports and perfect reverse isolation. These amplifiers can be implemented in four-port, four-mode systems with properly arranged two-mode squeezing and frequency-conversion couplings between the modes. The *T* amp, which has frequency-conversion coupling between its input and all the other modes, gives superior operating bandwidth compared to both single-pump parametric amplifiers and three-port directional amplifiers based on multiparametric couplings [6–8]. The *C* amp, with all its ports being matched, is robust against impedance mismatch on its auxiliary ports in practical operating conditions. Although these coupling schemes suggest that six couplings are needed to implement such amplifiers, the number of active parametric couplings can be reduced by employing frequency degeneracy among the four modes such that passive frequency-conversion couplings between these modes always exists. This method has been used in the implementation of directional devices in both optomechanical systems [16,22] and superconducting circuits [9,23,31]. These four-port, four-mode amplifiers are suitable for direct integration with superconducting circuits, and high-efficiency readout of large-scale superconducting qubits.

ACKNOWLEDGMENTS

We acknowledge helpful discussions with Wei Dai, Alessandro Miano, and Freek Ruesink. This research was sponsored by the Army Research Office (ARO) under Grants No. W911NF-18-1-0212, No. W911NF-16-1-0349, and No. W911NF-23-1-0051, and by the U.S. Department of Energy, Office of Science, National Quantum Information Science Research Centers, Co-design Center

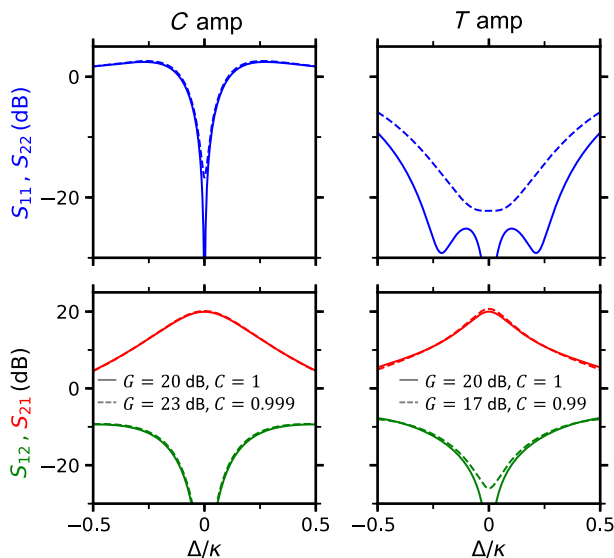


FIG. 5. Bandwidth of *C* amp and *T* amp. Bandwidth (B) of scattering matrix elements for (a) *C* amp and (b) *T* amp as a function of gain coupling strength G in the case of perfect conversion couplings ($C = 1$) between modes. The bandwidth of each scattering matrix elements is defined as the frequency range over which the corresponding condition is satisfied. The dot-dashed line represents the bandwidth of forward gain ($|S_{21}|^2 \leq G/2$) of a two-port phase-preserving amplifier.

for Quantum Advantage (C2QA) under Contract No. DE-SC0012704. The views and conclusions contained in this document are those of the authors and should not be interpreted as representing the official policies, either expressed or implied, of the U.S. Government. The U.S. Government is authorized to reproduce and distribute reprints for Government purposes notwithstanding any copyright notation herein.

-
- [1] J. E. Johnson, E. M. Hoskinson, C. Macklin, D. H. Slichter, I. Siddiqi, and John Clarke, Dispersive readout of a flux qubit at the single-photon level, *Phys. Rev. B* **84**, 220503 (2011).
 - [2] D. Ristè, J. G. van Leeuwen, H.-S. Ku, K. W. Lehnert, and L. DiCarlo, Initialization by measurement of a superconducting quantum bit circuit, *Phys. Rev. Lett.* **109**, 050507 (2012).
 - [3] Evan Jeffrey, Daniel Sank, J. Y. Mutus, T. C. White, J. Kelly, R. Barends, Y. Chen, Z. Chen, B. Chiaro, A. Dunsworth, A. Megrant, P. J. J. O’Malley, C. Neill, P. Roushan, A. Vainsencher, J. Wenner, A. N. Cleland, and John M. Martinis, Fast accurate state measurement with superconducting qubits, *Phys. Rev. Lett.* **112**, 190504 (2014).
 - [4] T. Walter, P. Kurpiers, S. Gasparinetti, P. Magnard, A. Potočnik, Y. Salathé, M. Pechal, M. Mondal, M. Oppliger, C. Eichler, and A. Wallraff, Rapid high-fidelity single-shot dispersive readout of superconducting qubits, *Phys. Rev. Appl.* **7**, 054020 (2017).
 - [5] Leonardo Ranzani and José Aumentado, A geometric description of nonreciprocity in coupled two-mode systems, *New J. Phys.* **16**, 103027 (2014).
 - [6] Leonardo Ranzani and José Aumentado, Graph-based analysis of nonreciprocity in coupled-mode systems, *New J. Phys.* **17**, 023024 (2015).
 - [7] K. M. Sliwa, M. Hatridge, A. Narla, S. Shankar, L. Frunzio, R. J. Schoelkopf, and M. H. Devoret, Reconfigurable Josephson circulator/directional amplifier, *Phys. Rev. X* **5**, 041020 (2015).
 - [8] F. Lecocq, L. Ranzani, G. A. Peterson, K. Cicak, R. W. Simmonds, J. D. Teufel, and J. Aumentado, Nonreciprocal microwave signal processing with a field-programmable Josephson amplifier, *Phys. Rev. Appl.* **7**, 024028 (2017).
 - [9] Baleegh Abdo, Nicholas T. Bronn, Oblesh Jinka, Salvatore Olivadese, Markus Brink, and Jerry M. Chow, Multi-path interferometric Josephson directional amplifier for qubit readout, *Quantum Sci. Technol.* **3**, 024003 (2018).
 - [10] F. Lecocq, L. Ranzani, G. A. Peterson, K. Cicak, A. Metelmann, S. Kotler, R. W. Simmonds, J. D. Teufel, and J. Aumentado, Microwave measurement beyond the quantum limit with a nonreciprocal amplifier, *Phys. Rev. Appl.* **13**, 044005 (2020).
 - [11] Baleegh Abdo, Oblesh Jinka, Nicholas T. Bronn, Salvatore Olivadese, and Markus Brink, High-fidelity qubit readout using interferometric directional Josephson devices, *PRX Quantum* **2**, 040360 (2021).
 - [12] A. Metelmann and A. A. Clerk, Nonreciprocal photon transmission and amplification via reservoir engineering, *Phys. Rev. X* **5**, 021025 (2015).
 - [13] A. Metelmann and A. A. Clerk, Nonreciprocal quantum interactions and devices via autonomous feedforward, *Phys. Rev. A* **95**, 013837 (2017).
 - [14] Freek Ruesink, Mohammad-Ali Miri, Andrea Alù, and Ewold Verhagen, Nonreciprocity and magnetic-free isolation based on optomechanical interactions, *Nat. Commun.* **7**, 13662 (2016).
 - [15] G. A. Peterson, F. Lecocq, K. Cicak, R. W. Simmonds, J. Aumentado, and J. D. Teufel, Demonstration of efficient nonreciprocity in a microwave optomechanical circuit, *Phys. Rev. X* **7**, 031001 (2017).
 - [16] Kejie Fang, Jie Luo, Anja Metelmann, Matthew H. Matheny, Florian Marquardt, Aashish A. Clerk, and Oskar Painter, Generalized non-reciprocity in an optomechanical circuit via synthetic magnetism and reservoir engineering, *Nat. Phys.* **13**, 465 (2017).
 - [17] N. R. Bernier, L. D. Tóth, A. Koottandavida, M. A. Ioannou, D. Malz, A. Nunnenkamp, A. K. Feofanov, and T. J. Kippenberg, Nonreciprocal reconfigurable microwave optomechanical circuit, *Nat. Commun.* **8**, 604 (2017).
 - [18] S. Barzanjeh, M. Wulf, M. Peruzzo, M. Kalaei, P. B. Dieterle, O. Painter, and J. M. Fink, Mechanical on-chip microwave circulator, *Nat. Commun.* **8**, 953 (2017).
 - [19] Freek Ruesink, John P. Mathew, Mohammad-Ali Miri, Andrea Alù, and Ewold Verhagen, Optical circulation in a multimode optomechanical resonator, *Nat. Commun.* **9**, 1798 (2018).
 - [20] Daniel Malz, László D. Tóth, Nathan R. Bernier, Alexey K. Feofanov, Tobias J. Kippenberg, and Andreas Nunnenkamp, Quantum-limited directional amplifiers with optomechanics, *Phys. Rev. Lett.* **120**, 023601 (2018).
 - [21] Laure Mercier de Lépinay, Erno Damskägg, Caspar F. Ockeloen-Korppi, and Mika A. Sillanpää, Realization of directional amplification in a microwave optomechanical device, *Phys. Rev. Appl.* **11**, 034027 (2019).
 - [22] Jason F. Herrmann, Vahid Ansari, Jiahui Wang, Jeremy D. Witmer, Shanhui Fan, and Amir H. Safavi-Naeini, Mirror symmetric on-chip frequency circulation of light, *Nat. Photonics* **16**, 603 (2022).
 - [23] Baleegh Abdo, Katrina Sliwa, S. Shankar, Michael Hatridge, Luigi Frunzio, Robert Schoelkopf, and Michel Devoret, Josephson directional amplifier for quantum measurement of superconducting circuits, *Phys. Rev. Lett.* **112**, 167701 (2014).
 - [24] Ofer Naaman and José Aumentado, Synthesis of parametrically coupled networks, *PRX Quantum* **3**, 020201 (2022).
 - [25] Carlton M. Caves, Quantum limits on noise in linear amplifiers, *Phys. Rev. D* **26**, 1817 (1982).
 - [26] See Supplemental Material at <http://link.aps.org/supplemental/10.1103/PhysRevApplied.21.014021> for detailed derivation and full scattering matrix.
 - [27] Tzu-Chiao Chien, *Creating Directional Quantum-Limited Amplification Using Multiparametric Devices* (University of Pittsburgh, Pittsburgh, PA, 2020).

- [28] N. Bergeal, R. Vijay, V. E. Manucharyan, I. Siddiqi, R. J. Schoelkopf, S. M. Girvin, and M. H. Devoret, Analog information processing at the quantum limit with a Josephson ring modulator, *Nat. Phys.* **6**, 296 (2010).
- [29] Low Noise Factory Inc, https://lownoisefactory.com/wp-content/uploads/2021/09/lnf-xxxxc4_8a-1.pdf.
- [30] QuinStar Technology, <https://quinstar.com/shop/cryogenic-products/cryogenic-circulators-isolators/cryogenic-circulators-qcy/>.
- [31] Randy Kwende, Theodore White, and Ofer Naaman, Josephson parametric circulator with same-frequency signal ports, 200 MHz bandwidth, and high dynamic range, *Appl. Phys. Lett.* **122**, 224001 (2023).